Title

Battery powered dual-polarity ion detector for trace chemical sensing

Authors

Fung, Stephanie
LeVasseur, Michael K
Rajapakse, Maneeshin Y
et al.

Publication Date

2022-05-01

DOI

10.1016/j.sna.2022.113442

Peer reviewed

Battery powered dual-polarity ion detector for trace chemical sensing

Stephanie Fung[1,2], Michael K. LeVasseur[1,2], Maneeshin Y. Rajapakse[1,2], Bradley S. Chew[1,2], Alexander G. Fung[1,2], Mitchell M. McCartney[1,2,3], Patrick Gibson[1], Nicholas J. Kenyon[1,2,3,4], Cristina E. Davis[1,2,3,*]

[1] Department of Mechanical and Aerospace Engineering, University of California Davis, Davis, CA, USA

[2] UC Davis Lung Center, One Shields Avenue, Davis, CA 95616, USA.

[3] VA Northern California Health Care System, 10535 Hospital Way, Mather, CA 95655, USA

[4] Department of Internal Medicine, University of California, Davis, 4150V Street, Suite 3400, Sacramento, CA 95817, USA

* Correspondence: cedavis@ucdavis.edu

Abstract

Trace chemical detection plays an important role in evaluating environmental hazards as well as benign chemical sources. We have developed a low power dual-polarity ionization-based detector. The detector electronics are operated with a single 9 V battery and provide concentration sensitive voltage outputs. The detection mode can be set manually with the on-board electronics or can be controlled with a microcontroller compatible digital input. The complete assembly and operation of the detector is detailed. The features of the detector make it suitable to be operated as a standalone system or to be integrated as a sub-system into a field-portable analytical platform. The detector can achieve a system step response of ~1.6 s. We performed laboratory measurements with several ionized chemicals using both positive and negative mode. The results showed highly linear responses at trace concentrations as low as 100 ppb.

Highlights:

- Low power ion detector with onboard controlled positive and negative mode detection suitable for integration into a portable microcontroller-based system
- Designed with commercially available off-the-shelf (COTS) components and can be operated using a standard 9 V battery
- Designed for low abundance ion detection, suitable for trace chemical VOCs

- As proof of concept, detection of photoionized chemicals at trace levels was performed

Keywords:
chemical sensor, portable chemical detection, low power, ion detection

1. Introduction

Trace chemical detection plays an important role in evaluating many types of environmental hazards as well as benign chemical sources. Volatile organic compounds (VOCs) in the air come from a variety of sources ranging from transportation emissions [1] to personal home care products [2,3]. In addition, toxic industrial chemicals and materials have widespread use in societies and are agents that may cause harm to humans when exposures occur [4]. Monitoring is often critical to ensure chemical concentrations do not exceed ambient exposure thresholds for each chemical set by the Environmental Protection Agency (EPA) in the United States. Advances in monitoring technologies are needed to detect and quantify these potentially harmful trace levels of chemicals. In addition to detecting potentially harmful chemicals, there are many biogenic VOCs of interest that present interesting detection applications such as non-invasive agriculture disease detection [5–10] and biogenic breath VOCs for health monitoring [5,11–13].

Traditionally, trace chemical detection in liquids and gasses is limited to laboratory environments. However, there are many potential applications where chemical detection in a field portable form factor would be advantageous [14]. For example, on-site screening for chemicals in emergency response scenarios could help emergency responders [15], and real-time industrial process monitoring in manufacturing environments could help ensure worker safety [16]. Current instrumentation for chemical detection frequently requires AC power along with additional computing infrastructure and a laboratory environment. This does not lend itself to remote sensing applications in varying locations or harsh environments. Currently for gold standard measurements, environmental samples are captured, stored, and transported back to the laboratory to perform detection and analysis. While there has been much work in preconcentration of samples to boost detection quantification ranges [17–20], robust portable chemical detectors are still needed to unlock advanced applications of chromatography in field applications [21–23].

Regardless of the instrumentation, the key to sensing ambient chemicals and VOCs of interest is to ionize the sample and detect the concentration. Many miniaturized trace chemical detectors have been developed in the recent decades [24–28]. Sensing trace chemicals <1 ppm results in current levels in the picoampere range, and the design of the fixturing and electronics to successfully detect such low levels is non-trivial. Previously reported detector electronics claim low power battery operation [29], but fail to show stability with battery operation conditions, report the expected total run-time, and the bias configuration.

Additionally, there is the charge polarity of the ion species to consider. Several analytical techniques can be used to detect ions from gas phase trace levels of chemicals [23,27,30,31]. Gas phase chemicals subject to an ionization source can generate both positive and negative ions. Detection of ions of both polarities is important in the application of hazardous trace chemical detection. Hazardous VOCs typically generate positive ions by different mechanisms at the ionization source such as loss of electrons or by adduct ion formation and must be detected by negatively biased detector [32]. In contrast, hazardous ordnance related compounds such as explosives can be only detected as negative ions with few exceptions. Sensing these compounds is achieved with aid of a dopant and making stable adduct ions such as chloride adducts. The resulting ions can survive several milliseconds in air at ambient pressure before being neutralized due to collisions. Therefore, it is necessary to have detection technologies that can match these timescales and amplify the low ion currents of both polarities to detect chemicals of interest.

Previous works have reported ionization methods and detection electronics in a piecemeal and ad hoc fashion. Few references provide the details needed to manufacture the detection apparatus. No study has been reported for a battery powered ion detection system with the capability to detect ions in both positive and negative modes. In this work, we report a dual-polarity portable ion detector powered from a standard 9 V battery. The detector was designed to be compact and low power such that it could be integrated into a mobile chemical sensing platform while providing performance that matches or exceeds that of a gold-standard benchtop instrument.

2. Materials and Methods

Our detector system is a combination of modules that together provide low power and trace detection of charged ion species for chemical sensing (Figure 1). The sensing component of the system is a microfabricated device called μDC (microfabricated detector channel) that detects charged ions (section 2.1). This device is housed within a custom designed fixture (section 2.2) which accommodates an ionization source and facilitates gas phase sample introduction. The complete system assembly is described (section 2.2). Finally, custom control and signal conditioning electronics are packaged on printed circuit boards (PCBs) (section 2.3). The entire device measures 50 mm x 55 mm x 25 mm. The system is powered by a 9 V battery, thus making it suitable for field portable applications.

2.1 Microfabricated detector channel (μDC)

2.1.1 Device Fabrication

The μDC devices (Figure 2) for this paper were fabricated with an updated modified manufacturing method similar to a device designed by our group and reported earlier [33]. The process steps were carried out in our campus Class 100 cleanroom facility (Center for Nano-MicroManufacturing, University of California Davis). The

starting substrate was a 100 mm round, 700 µm thick borosilicate glass wafer (Borofloat 33; Schott North America, Inc., Louisville, KY). An electron beam (CHA Industries AutoTech II, Fremont, CA) was used to deposit thin film layers of conductive Cr and Au having thickness of 20 and 100 nm respectively. Briefly, NR9-1500PY negative photoresist (Futurrex Inc., Franklin, NJ) was spun onto the wafer at 3000 rpm, and soft baked at 150 °C for 3.5 minutes. Photolithography was performed using a Karl-Suss M4A mask aligner with flood exposure at 15 mW/cm^2 for 24 seconds to define the electrodes using a full contact transparency mask (CAD/Art Services, Inc., Bandon, OR). A post-exposure bake of 100°C for 3.5 minutes was followed by development for 20 seconds in RD6 developer solution (Futurrex Inc., Franklin, NJ). A hard-bake was then performed at 130 °C for 3 minutes. The pattern was etched into the metal layers with a solution of diluted aqua regia (3:1:10 $HCl:HNO_3:H_2O$), followed by an etch in Cr etchant 1020 (Transene Company, Inc., Danvers, MA). Following removal of the photoresist in a sonicated solution of RR41 resist remover (Futurrex Inc., Franklin, NJ), dicing of the wafer created rectangular chip halves with symmetric electrodes.

The mask aligner and a programmable furnace (Naytech,Vulcan 3-550) were used to form the gas flow path of the µDC device. Placing a strip of laminated polyimide film, 500FN131 (Dupont, Wilmington, DE), between two previously patterned glass chips, a temporary bond was set with the mask aligner, matching the locations of the top and bottom detector electrodes. The device was then transferred to the programmable furnace where it was thermally bonded at 210 °C for 15 minutes with an applied pressure of 5 psi.

2.1.2 Device Operation

The detector channel dimensions are defined with the fabrication process whereby the laminated film acts as a spacer and determines the height and width of the channel that is formed (Figure 2). The inlet and outlet to the µDC is the slit formed at each end of the bonded device. Ionized sample flows into the chip at the inlet which is closest to the detector electrodes. The sample continues through the channel to the outlet slit where it can be properly exhausted or continue to be analyzed by other methods.

At the device inlet, there are two detector electrodes, with dimensions 5.00 x 10.75 mm, patterned on each of the chip halves that run parallel to each other along the formed channel. More details on the device dimensions can be found in Supplemental Figure 1. Each detector electrode is biased to either a positive or negative voltage using the electronics discussed in (section 2.3). The function of the biased voltage is two-fold: first the biased voltage acts to attract the ion of the opposite charge to the sensing electrode, second the electrode directly opposite deflects the ions of the same charge to the appropriate sensing electrode. Ions neutralizing on the detection electrode generate a current proportional to the concentration of the ionized chemical in the sample. The bias electrode is set to the respective bias voltage and serves as an on-chip guard ring to minimize current leakage from the detector electrode. Patterned metal traces leading to metal pads on the device provide an electrical interface to the electrodes that are accessible through an opening in the fixture.

2.2 System Assembly

The μDC is housed in a metal fixture with the complete assembly process shown (Figure 1). The device is clamped tightly in place between two silicone gaskets in an aluminum housing, which provides electrical shielding and structural integrity. The flow paths into and out of the device are sealed with laser-cut Viton gaskets. These are mated with the aluminum inlet and outlet blocks and are aligned with precision stainless steel dowel pins and held with fasteners. The PCBs are designed such that spring metal pins contacts (Mill-Max, Oyster Bay, NY) fit precisely through slots in the metal fixture to make an electrical connection to the corresponding electrode pads on the device. Additionally, a copper shielding plate is mounted above the circuit boards to provide additional shielding. The ionization source is installed on the inlet block over the ionization chamber and sealed with a standard O-ring. Gas flow connections are made at the inlet and outlet via standard 10-32 thread fittings.

Sample Introduction and Ionization

The cross section view shows the detail of the sample flow path through the system (Figure 3). Sample is introduced into the inlet block which has machined 10-32 threads for using standard tube fitting adapters. A machined opening in the inlet block serves as an ionization chamber where the sample is ionized with a 10.6 eV Kr UV bulb (Analytical West, Corona, CA). Photoionization was utilized for the experiments carried out in this article, but it is possible to adapt this fixture for alternative ionization sources with higher energy potentials such as Ni-63 (radioactive), corona discharge, or other advanced ionization method. Directly following ionization, the sample enters the μDC.

2.3 Electronics Architecture

The detector system electronics are comprised of two symmetric printed circuit boards mounted on each side of the fixture. This two PCB system facilitates a highly configurable ion detection platform allowing for positive and negative mode ion sensing either independently or simultaneously. For the most versatility, there are physical jumper pins that allow the bias voltage of the PCB to be set to be negative, positive, ground, or digital mode. The digital mode setting enables microcontroller control of the voltage bias and thus enabling remote control of the detector operation mode. The digital mode is facilitated by using a switch package (Texas Instruments, Dallas, TX) that is compatible with both 3.3 and 5 V digital control inputs covering the great majority of readily available microcontroller platforms. The circuit is illustrated in Supplemental Figure 2.

Battery Power

For the electronics to function off battery power, a power system was designed to supply the sensitive components with very low noise voltage. The architecture of the power network fully powered off one 9 V battery is shown in Supplemental Figure 3. The step-up/down regulator S18V20F9 (Pololu, Las Vegas, NV) ensures a stable voltage as battery voltage can vary from battery to battery and throughout the life of a single battery as the voltage tends to decrease as it nears empty (Table 1.). A DC/DC converter allows for negative voltages that are subsequently regulated with low-noise LDO (low-dropout) regulators that provide extremely stable voltage

supplies for the integrated circuit (IC) device on the PCB and for the bias voltages as well. The resulting current draw of the system is approximately 25 mA. Given that the capacity of 9 V batteries is typically around 500 mAh, the system can easily last an entire day of non-stop field work and could potentially last over several days with intermittent operation.

Signal Conditioning

Currents from trace chemical concentrations are often in the picoamp and as low as the femtoampere range. The device is surrounded by the grounded metal fixture to minimize electrical noise from the environment. The amplification electronics for the detector module is arranged in two stages as depicted in Supplemental Figure 4. The first stage is comprised of a transimpedance amplifier with an extremely high gain set by the gain resistor RH73X2A50GNTN (TE Connectivity, Schaffhausen, Switzerland). The PCB layout of this stage is critical to minimize leakage current paths. The input current path (Figure 4) to the operational amplifier is surrounded by a guard trace that is held to the bias voltage level. Furthermore, that area is void of soldermask to eliminate a possible leakage current path. After the PCBs are assembled, they are cleaned in an ultrasonic bath with saponifying cleaner to remove any residue such as flux that may also act as a leakage path.

The second stage uses an instrumentation amplifier to further amplify the converted voltage signal and to remove the bias voltage from the output. The gain of the instrumentation amplifier INA188 (Texas Instruments, Dallas, Texas) is set by a single external resistor and can be set from 1 to 1000. In the reported experiments, the gain of the second stage was set to 6. This additional signal conditioning also helps for measuring the output either with a handheld digital multimeter or for integration into a microcontroller-based system. Such electronics are highly sensitive to electromagnetic interference (EMI) so a grounded copper shield is mounted above the PCBs to further shield the circuitry.

3. Results and Discussion

The setup to measure trace chemicals with the detector is shown (Figure 5). House compressed air is filtered (Restek, Bellafonte, PA) and serves as the carrier gas. The air is metered at 200 mL/min using a mass flow controller (Alicat Scientific, Tuscon, AZ). The carrier flow is combined with the sample at a tee (Swagelok, Solon, OH). Chemical samples were prepared [34] at 1000 ppm for each chemical species in a Tedlar gas sampling bag (Sigma-Aldrich, St. Louis, MO). A gas tight 10 mL syringe (Hamilton Company, Reno, NV) is filled with the sample and the flow is metered with a syringe pump (Harvard Apparatus, Holliston, MA) to augment the resulting trace concentration of the chemical that comes out of the tee. Keeping the carrier gas flow constant, chemical sample with varied concentrations ranging from were injected into the detector system. Directly at the outlet of the tee, the mixed sample and carrier gas is transported with a heated stainless steel metal tubing line. A temperature controller (Omega Engineering Inc., Norwalk, CT) with PID control was

used to achieve the gas heating with a setpoint of 90 °C. Usually higher temperature fluctuations will affect ion mobility based chemical results and signal intensity. However, we kept the temperature at a stable level by allowing the detector assembly with the carrier gas to stabilize at an experimented temperature with the control of the temperature of the heated inlet line. Signals were reproducible with such conditions. Usually, temperature fluctuations of ±2 degree or less contribute negligible impact to an ion mobility chemical signal and its intensity [35]. Our data were obtained within those limits. Prior to testing with chemical samples, the entire module was leak tested with helium gas at 10 mL/min to ensure that there was flow through the sensing device and to prevent any hazardous chemicals from leaking into the environment.

3.1 System Step Response

To measure the step input response of the system, 1 ppm acetone was injected at a constant rate. Then at manually controlled intervals, the ionization source (UV) was switched on resulting in the rise shown in and kept on until a steady state is reached and then switched off. This was repeated for four replicates. One of the replicates is plotted and shown in Figure 6. The response time was then calculated as time elapsed to reach a signal value -3dB from the stabilized maximum value. The step response time constant τ was found to be 1.6 seconds. This is nearly half the value of the battery operated electrometer reported in [29] where the step response was measured in an ideal configuration.

3.2 Detection of Trace Chemicals in Dual Polarities

The linearity and detection capability of the system was examined for several chemicals. The syringe pump volume flow was varied to produce different concentrations ranging from 100 to 10000 ppb while keeping the carrier gas flow constant at 200 mL/min. Injections were performed for several positive mode (toluene, xylene and acetone) and negative mode (acetone and methyl salicylate) chemicals. The injections for each concentration were performed in triplicate (n=3). Due to background noise and other environmental factors, there is an offset in the signal that results a non-zero baseline value. This can be automatically corrected by taking a baseline measurement that can then be used to subtract from subsequent measurements. The positive mode chemicals (Figure 7) were each measured at the same corresponding concentrations from 100 to 750 ppb and the results show highly linear responses. The negative mode responses for acetone and methyl salicylate were also highly linear. Methyl salicylate was found to have a much lower amplitude of signal to concentration ratio compared to acetone. The results of the negative mode responses are plotted separately (Figure 8). The response of Acetone was measured at concentrations from 100 to 1000 ppb and showed highly linear responses like that of the positive mode measurements. Methyl salicylate was measured at concentrations from 250 to 10000 ppb. The results are still highly linear but less than that of measurements taken from a smaller range of concentrations which is to be expected. This illustrates the potential for this system to be used for detection of a wide range of concentrations.

4. Conclusion

A low powered dual-polarity portable ion detector was developed and demonstrated to detect trace level chemicals. The detector electronics allow for both manual and digital control of the ion sensing polarity mode. Ion species of both positive and negative polarity were sensed at trace levels down to 100 ppb. The output of the detector in both modes showed linear responses proportional to the chemical concentrations tested. Future work will explore the great promise in integrating this detector in series with other analytical techniques such as GC and IMS to add dimensionality to the analysis. The low current draw and small form factor is amenable for integrating into field portable systems. Furthermore, with the integration of a desorption unit and the use of a higher energy ionization source, the detection of negative ion yielding compounds, such as explosives, may be explored.

5. Acknowledgements

This work was partially supported by: NIH NCATS 1U18TR003795-01 [CED, NJK] and UL1 TR001860 [CED, NJK]; NIH award UG3-OD023365 [CED, NJK]; NIH award 1P30ES023513-01A1 [CED, NJK]; University of California CITRIS and the Banatao Institute award 19-0092 [CED, NJK]; the Department of Veterans Affairs award I01 BX004965-01A1 [CED, NJK]; and the University of California Tobacco-Related Disease Research Program award T31IR1614 [CED, NJK]. Part of this study was carried out at the UC Davis Center for Nano and Micro Manufacturing (CNM2). The contents of this manuscript are solely the responsibility of the authors and do not necessarily represent the official views of the funding agencies.

6. Competing Interests Statement

The authors declare no conflicts of interest.

The authors declare no competing financial interest. The software code and PCB design specifications for our sampling device are available on GitHub. Please refer to Professor Cristina Davis' webpage for more information. Future published scientific manuscripts or reports using this software and/or hardware designs must cite this original publication (DOI: xxxxxxxxx).

7. Author Statement

Stephane Fung: conceptualization, design and analysis, experiment planning, experimental data, review of data and results, writing original draft, writing review and editing. **Michael LeVasseur**: conceptualization, design and analysis, experiment planning, experimental data, review of data and results, writing original draft, writing review and editing. **Maneeshin Rajapakse**: conceptualization, design and analysis, experiment planning, experimental data, review of data and results, writing original draft, writing review and editing. **Bradley Chew**: conceptualization, design and analysis, experiment planning, experimental data, review of data and results, writing original draft, writing review and editing. **Alexander Fung**: conceptualization, design and analysis, experiment planning, experimental data, review of data and results, writing original draft, writing review and editing. **Mitchell McCartney**: conceptualization, design and analysis, experiment planning, review of data and results, writing original draft, writing review and editing. **Patrick Gibson**: conceptualization, experiment planning, review of data and results, writing review and editing. **Nicholas Kenyon**: conceptualization, funding, mentoring and supervision, writing review and editing. **Cristina Davis**: conceptualization, experiment planning, review of data and results, funding, mentoring and supervision, writing original draft, writing review and editing.

8. References

[1] D.R. Gentner, S.H. Jathar, T.D. Gordon, R. Bahreini, D.A. Day, I. El Haddad, P.L. Hayes, S.M. Pieber, S.M. Platt, J. de Gouw, A.H. Goldstein, R.A. Harley, J.L. Jimenez, A.S.H. Prévôt, A.L. Robinson, Review of Urban Secondary Organic Aerosol Formation from Gasoline and Diesel Motor Vehicle Emissions, Environ. Sci. Technol. 51 (2017) 1074–1093. https://doi.org/10.1021/acs.est.6b04509.

[2] B.C. McDonald, J.A. de Gouw, J.B. Gilman, S.H. Jathar, A. Akherati, C.D. Cappa, J.L. Jimenez, J. Lee-Taylor, P.L. Hayes, S.A. McKeen, Y.Y. Cui, S.-W. Kim, D.R. Gentner, G. Isaacman-VanWertz, A.H. Goldstein, R.A. Harley, G.J. Frost, J.M. Roberts, T.B. Ryerson, M. Trainer, Volatile chemical products emerging as largest petrochemical source of urban organic emissions, Science (80-.). 359 (2018) 760–764. https://doi.org/10.1126/science.aaq0524.

[3] M.M. Rahman, K.-H. Kim, Potential hazard of volatile organic compounds contained in household spray products, Atmos. Environ. 85 (2014) 266–274. https://doi.org/10.1016/j.atmosenv.2013.12.001.

[4] U.B. Nurmatov, N. Tagieva, S. Semple, G. Devereux, A. Sheikh, Volatile organic compounds and risk of asthma and allergy: a systematic review and meta-analysis of observational and interventional studies, Prim. Care Respir. J. 2013 221. 22 (2013) S9–S15. https://doi.org/10.4104/pcrj.2013.00010.

[5] M.M. Elmassry, M.A. Farag, In Vivo and In Vitro Volatile Organic Compounds (VOCs) Analysis in Bacterial Diagnostics: Case Studies in Agriculture and Human Diseases, Bact. Volatile Compd. as Mediat. Airborne Interact. (2020) 123–138. https://doi.org/10.1007/978-981-15-7293-7_4.

[6] A. Pasamontes, W.H.K. Cheung, J. Simmons, A.A. Aksenov, D.J. Peirano, E.E. Grafton-Cardwell, T. Kapaun, A.M. Dandekar, O. Fiehn, C.E. Davis, Citrus tristeza virus infection in sweet orange trees and a mandarin × tangor cross alters low molecular weight metabolites assessed using gas chromatography mass spectrometry (GC/MS), Metabolomics 2016 123. 12 (2016) 1–10. https://doi.org/10.1007/S11306-016-0959-Z.

[7] W.H.K. Cheung, A. Pasamontes, D.J. Peirano, W. Zhao, E.E. Grafton-Cardwell, T. Kapaun, R.K. Yokomi, J. Simmons, M. Doll, O. Fiehn, A.M. Dandekar, C.E. Davis, Volatile organic compound (VOC) profiling of citrus tristeza virus infection in sweet orange citrus varietals using thermal desorption gas chromatography time of flight mass spectrometry (TD-GC/TOF-MS), Metabolomics 2015 116. 11 (2015) 1514–1525. https://doi.org/10.1007/S11306-015-0807-6.

[8] C.H. Thompson, M.M. McCartney, T. V. Roubtsova, T. Kasuga, S.E. Ebeler, C. Davis, R.M. Bostock, Analysis of Volatile Profiles for Tracking Asymptomatic Infections of *Phytophthora ramorum* and other pathogens in *Rhododendron*, Phytopathology®. (2021) PHYTO-10-20-0472-R. https://doi.org/10.1094/PHYTO-10-20-0472-R.

[9] M.M. McCartney, T. V. Roubtsova, M.S. Yamaguchi, T. Kasuga, S.E. Ebeler, C.E. Davis, R.M. Bostock, Effects of Phytophthora ramorum on volatile organic compound emissions of Rhododendron using gas chromatography–mass spectrometry, Anal. Bioanal. Chem. 2017 4105. 410 (2017) 1475–1487. https://doi.org/10.1007/S00216-017-0789-5.

[10] R.M.C. Jansen, J.W. Hofstee, J. Wildt, B.H.E. Vanthoor, F.W.A. Verstappen, K. Takayama, H.J. Bouwmeester, E.J. van Henten, Health monitoring of plants by their emitted volatiles: A model to predict the effect of Botrytis cinerea on the concentration of volatiles in a large-scale greenhouse, Biosyst. Eng. 106 (2010) 37–47. https://doi.org/10.1016/j.biosystemseng.2010.01.009.

[11] A.A. Aksenov, L. Yeates, A. Pasamontes, C. Siebe, Y. Zrodnikov, J. Simmons, M.M. McCartney, J.-P. Deplanque, R.S. Wells, C.E. Davis, Metabolite Content Profiling of Bottlenose Dolphin Exhaled Breath, Anal. Chem. 86 (2014) 10616–10624. https://doi.org/10.1021/ac5024217.

[12] R. Cumeras, W.H.K. Cheung, F. Gulland, D. Goley, C.E. Davis, Chemical Analysis of Whale Breath Volatiles: A Case Study for Non-Invasive Field Health Diagnostics of Marine Mammals, Metab. 2014, Vol. 4, Pages 790-806. 4 (2014) 790–806. https://doi.org/10.3390/METABO4030790.

[13] A.T. Güntner, S. Abegg, K. Königstein, P.A. Gerber, A. Schmidt-Trucksäss, S.E. Pratsinis, Breath Sensors for Health Monitoring, ACS Sensors. 4 (2019) 268–

280. https://doi.org/10.1021/ACSSENSORS.8B00937.

[14] O.A.M. Popoola, D. Carruthers, C. Lad, V.B. Bright, M.I. Mead, M.E.J. Stettler, J.R. Saffell, R.L. Jones, Use of networks of low cost air quality sensors to quantify air quality in urban settings, Atmos. Environ. 194 (2018) 58–70. https://doi.org/10.1016/j.atmosenv.2018.09.030.

[15] A.J. Caban-Martinez, B. Kropa, N. Niemczyk, K.J. Moore, J. Baum, N.S. Solle, D.A. Sterling, E.N. Kobetz, The “Warm Zone” Cases: Environmental Monitoring Immediately Outside the Fire Incident Response Arena by Firefighters, Saf. Health Work. 9 (2018) 352–355. https://doi.org/10.1016/j.shaw.2017.12.003.

[16] A. Gałuszka, Z.M. Migaszewski, J. Namieśnik, Moving your laboratories to the field – Advantages and limitations of the use of field portable instruments in environmental sample analysis, Environ. Res. 140 (2015) 593–603. https://doi.org/10.1016/j.envres.2015.05.017.

[17] M.Y. Rajapakse, E. Borras, A.G. Fung, D. Yeap, M.M. McCartney, F.M. Fabia, N.J. Kenyon, C.E. Davis, An environmental air sampler to evaluate personal exposure to volatile organic compounds, Analyst. 146 (2021) 636–645. https://doi.org/10.1039/D0AN01521K.

[18] A.G. Fung, M.Y. Rajapakse, M.M. Mccartney, A.K. Falcon, F.M. Fabia, N.J. Kenyon, C.E. Davis, Wearable Environmental Monitor To Quantify Personal Ambient Volatile Organic Compound Exposures, ACS Sensors. 4 (2019) 1358–1364. https://doi.org/10.1021/acssensors.9b00304.

[19] M.M. McCartney, Y. Zrodnikov, A.G. Fung, M.K. Levasseur, J.M. Pedersen, K.O. Zamuruyev, A.A. Aksenov, N.J. Kenyon, C.E. Davis, An Easy to Manufacture Micro Gas Preconcentrator for Chemical Sensing Applications, ACS Sensors. 2 (2017) 1167–1174. https://doi.org/10.1021/acssensors.7b00289.

[20] N. Strand, A. Bhushan, M. Schivo, N.J. Kenyon, C.E. Davis, Chemically polymerized polypyrrole for on-chip concentration of volatile breath metabolites, Sensors Actuators B Chem. 143 (2010) 516–523. https://doi.org/10.1016/j.snb.2009.09.052.

[21] S. Zampolli, I. Elmi, G.C. Cardinali, L. Masini, F. Bonafè, F. Zardi, Compact-GC platform: A flexible system integration strategy for a completely microsystems-based gas-chromatograph, Sensors Actuators B Chem. 305 (2020) 127444. https://doi.org/10.1016/j.snb.2019.127444.

[22] R.R.A. Syms, S. Wright, MEMS mass spectrometers: the next wave of miniaturization, J. Micromechanics Microengineering. 26 (2016) 023001. https://doi.org/10.1088/0960-1317/26/2/023001.

[23] A.T. Kirk, M. Allers, P. Cochems, J. Langejuergen, S. Zimmermann, A compact high resolution ion mobility spectrometer for fast trace gas analysis, Analyst. 138 (2013) 5200. https://doi.org/10.1039/c3an00231d.

[24] S. Weigl, F. Feldmeier, R. Bierl, F.-M. Matysik, Photoacoustic detection of acetone in N2 and synthetic air using a high power UV LED, Sensors Actuators B Chem. 316 (2020) 128109. https://doi.org/10.1016/j.snb.2020.128109.

[25] S. Narayanan, G. Rice, M. Agah, A micro-discharge photoionization detector for micro-gas chromatography, Microchim. Acta. 181 (2014) 493–499. https://doi.org/10.1007/s00604-013-1146-9.

[26] P. Intra, N. Tippayawong, Development and Evaluation of a Faraday Cup Electrometer for Measuring and Sampling Atmospheric Ions and Charged Aerosols, Part. Sci. Technol. 33 (2015) 257–263. https://doi.org/10.1080/02726351.2014.952392.

[27] M. Wei-Hao Li, A. Ghosh, A. Venkatasubramanian, R. Sharma, X. Huang, X. Fan, High-Sensitivity Micro-Gas Chromatograph–Photoionization Detector for Trace Vapor Detection, ACS Sensors. 6 (2021) 2348–2355. https://doi.org/10.1021/acssensors.1c00482.

[28] S.O. Agbroko, J. Covington, A novel, low-cost, portable PID sensor for the detection of volatile organic compounds, Sensors Actuators B Chem. 275 (2018) 10–15. https://doi.org/10.1016/j.snb.2018.07.173.

[29] M. He, P. Marzocca, S. Dhaniyala, A new high performance battery-operated electrometer, Rev. Sci. Instrum. 78 (2007) 105103. https://doi.org/10.1063/1.2789659.

[30] W. Wang, S. Wang, C. Xu, H. Li, Y. Xing, K. Hou, H. Li, Rapid Screening of Trace Volatile and Nonvolatile Illegal Drugs by Miniature Ion Trap Mass Spectrometry: Synchronized Flash-Thermal-Desorption Purging and Ion Injection, Anal. Chem. 91 (2019) 10212–10220. https://doi.org/10.1021/acs.analchem.9b02309.

[31] G.. Eiceman, B. Tadjikov, E. Krylov, E.. Nazarov, R.. Miller, J. Westbrook, P. Funk, Miniature radio-frequency mobility analyzer as a gas chromatographic detector for oxygen-containing volatile organic compounds, pheromones and other insect attractants, J. Chromatogr. A. 917 (2001) 205–217. https://doi.org/10.1016/S0021-9673(01)00656-2.

[32] G.A. Eiceman, Z. Karpas, H.H. Hill Jr., Ion Mobility Spectrometry, CRC Press, 2013. https://doi.org/10.1201/b16109.

[33] Y. Zrodnikov, M.Y. Rajapakse, D.J. Peirano, A.A. Aksenov, N.J. Kenyon, C.E. Davis, High Asymmetric Longitudinal Field Ion Mobility Spectrometry Device for Low Power Mobile Chemical Separation and Detection, Anal. Chem. 91 (2019) 5523–5529. https://doi.org/10.1021/acs.analchem.8b05577.

[34] D. Yeap, P.T. Hichwa, M.Y. Rajapakse, D.J. Peirano, M.M. McCartney, N.J. Kenyon, C.E. Davis, Machine Vision Methods, Natural Language Processing, and Machine Learning Algorithms for Automated Dispersion Plot Analysis and Chemical Identification from Complex Mixtures, Anal. Chem. 91 (2019) 10509–

10517. https://doi.org/10.1021/acs.analchem.9b01428.

[35] M. Y. Rajapakse, J. A. Stone, G. A. Eiceman, Decomposition Kinetics of Nitroglycerine·Cl–(g) in Air at Ambient Pressure with a Tandem Ion Mobility Spectrometer, J. Phys. Chem. A. 118 (2014) 2683–2692. https://doi.org/10.1021/jp412444b.

9. Figures

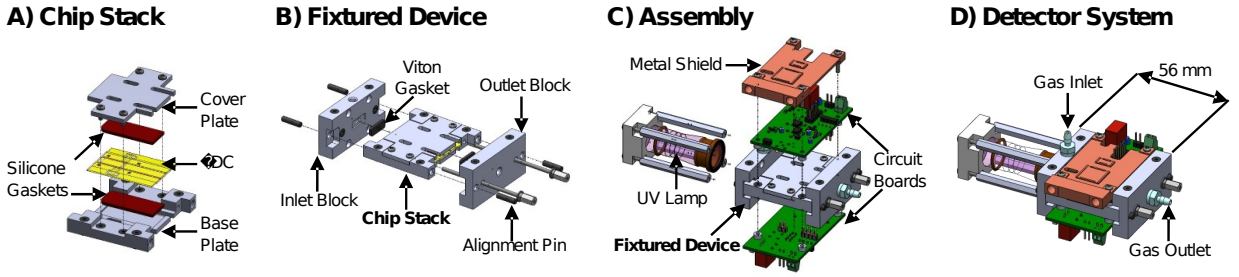

Figure 1: The chemical detection system is a combination of component modules that together allow for trace positive and negative charged ion detection. (A) The device is sandwiched in a stack held in place with two silicone gaskets compressed by metal cover and base plates. (B) The chip stack is fixtured between two metal blocks with Viton gaskets at the inlet and outlet to create an airtight seal. (C) Electronics and ionization source attach to the fixtured device and are interchangeable to meet application needs. (D) Fully assembled detector system.

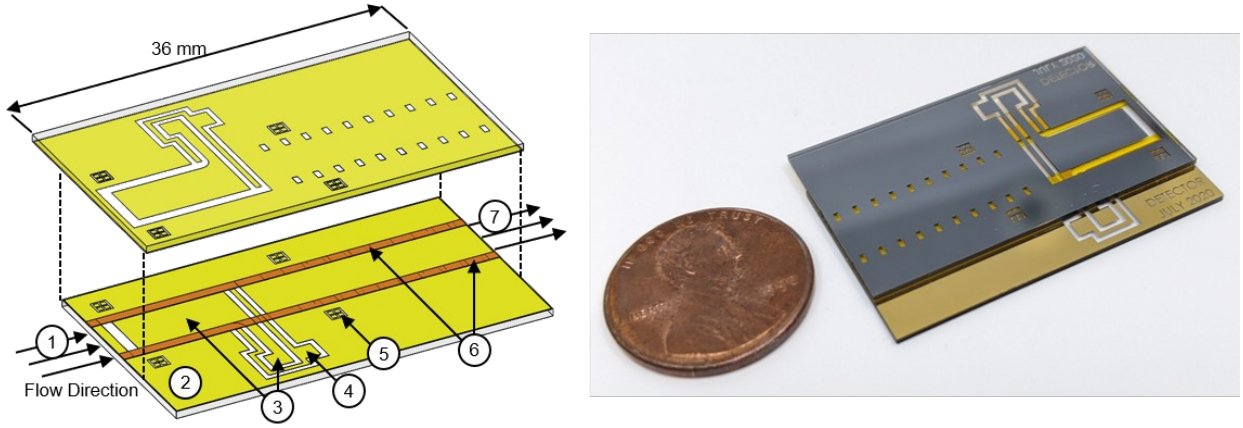

Figure 2. Microfabricated detector channel (μDC) is manufactured on a borosilicate substrate using standard photolithography and etch techniques detailed in Section 13

2.1.1. (1) Inlet to the chip; (2) Patterned metal ground plane; (3) The detector electrode and trace leading out to the pad; (4) Bias voltage surrounds the detector electrode on the chip to guard against leakage current; (5) Alignment markers; (6) Polyimide spacers that define the channel dimensions; (7) The device outlet. A photograph of the assembled device is shown next to a US penny to provide scale.

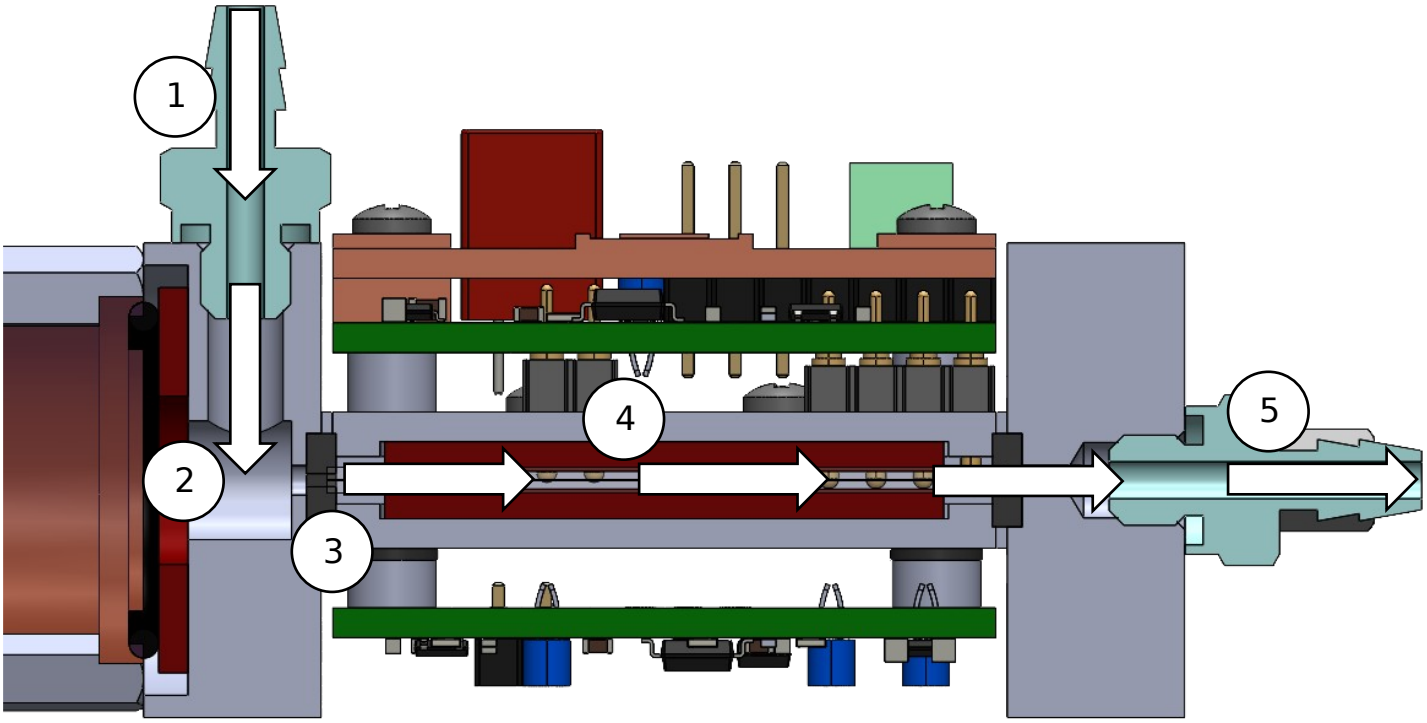

Figure 3. (1) Side cross section view of the assembled Detector detailing the flow path; (2) Sample gas is introduced at the inlet; (3) The sample is then ionized by the UV bulb; (4) Ionized sample flows into the device; (5) Ion species are attracted to their respective detector electrode and ion neutralization induces a current that is converted into a voltage signal by the circuitry; (6) Sample exits the device through the outlet.

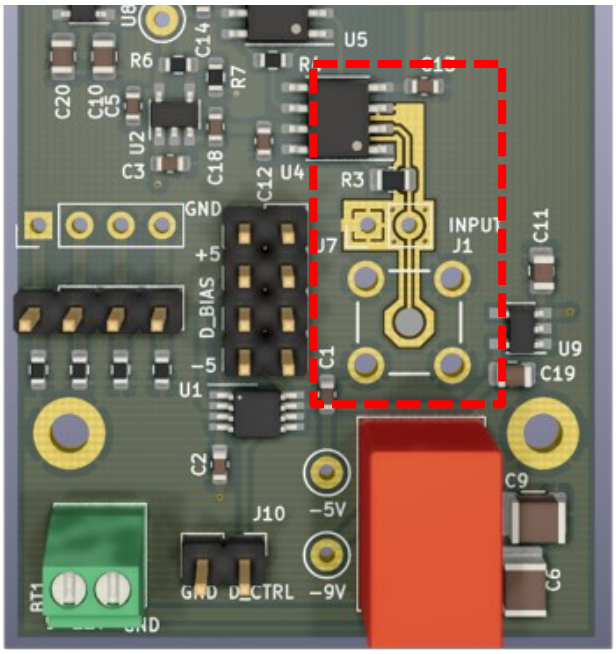

Figure 4. Rendering of the detector electronics PCB highlighting the guarded signal input path

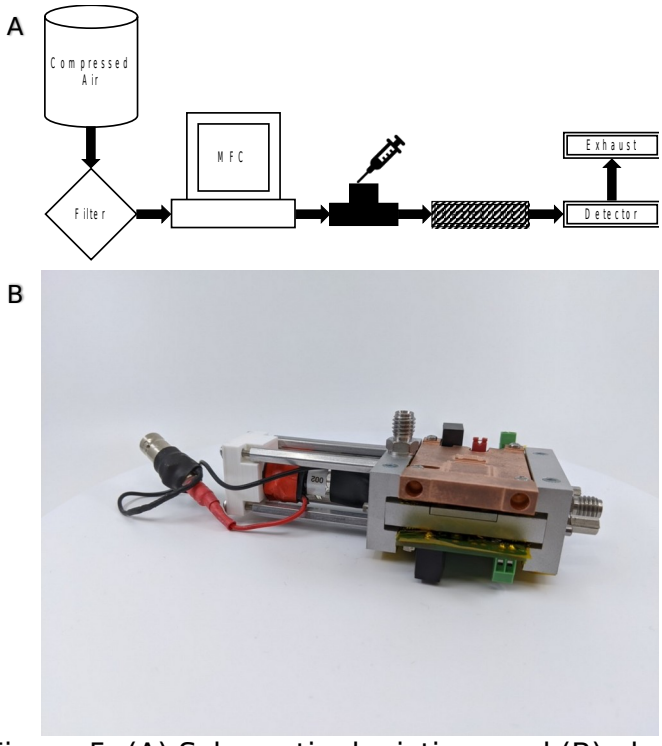

Figure 5. (A) Schematic depiction, and (B) photograph of the assembled detector.

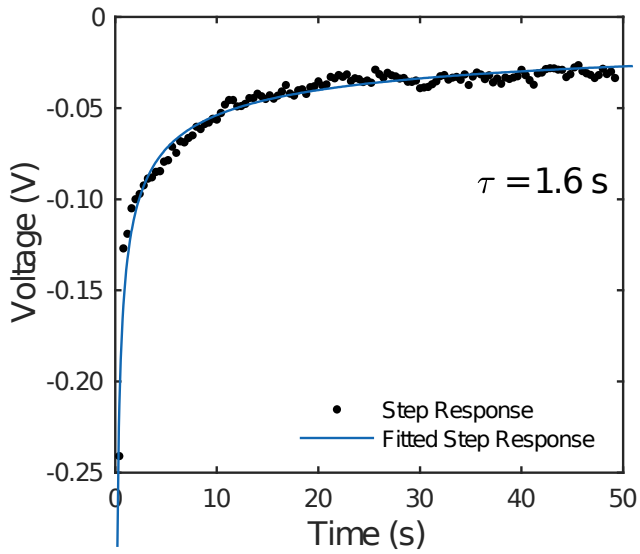

Figure 6. Detector output response to step input

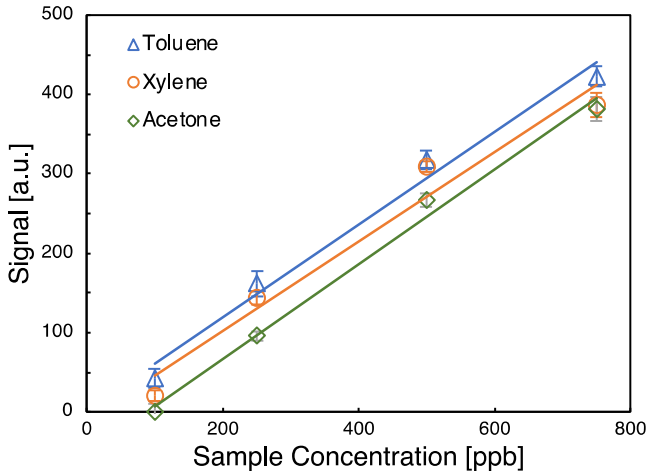

Figure 7. Signal response in a.u. (arbitrary units) for positive mode chemicals versus the concentration (100, 250, 500, and 750 ppb). The R^2 values are 0.98, 0.97, and 0.99 for toluene, xylene, and acetone respectively. Vertical error bars represent the standard deviation of three replicates.

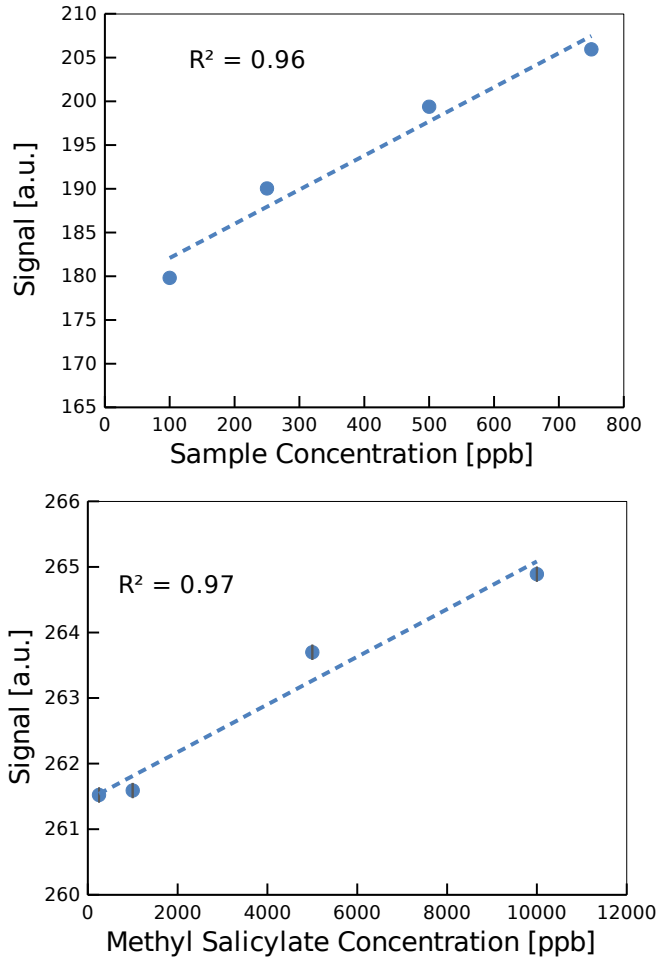

Figure 8. Signal response for negative mode detection of two chemicals. Top panel shows linearity for acetone. Bottom panel shows signal at a much wider range of concentration still has a linear trend. The signal response slope with increasing concentration for methyl salicylate in negative mode detection was significantly lower than acetone.

10. Tables

Table 1. Current draw, baseline average taken over a 10 second interval, and standard deviation presented for a range of supply voltages to simulate battery voltage level fluctuations.

Supply (V)	Current (mA)	Baseline (V)	□
7.50	26.8	6.185	0.0048
7.75	26.4	6.190	0.0048
8.00	26.0	6.193	0.0056
8.25	25.6	6.185	0.0042
8.50	25.3	6.184	0.0043
8.75	24.9	6.191	0.0053
9.00	24.5	6.187	0.0042
9.25	24.2	6.186	0.0057
9.50	23.8	6.184	0.0043

11. Supplementary material

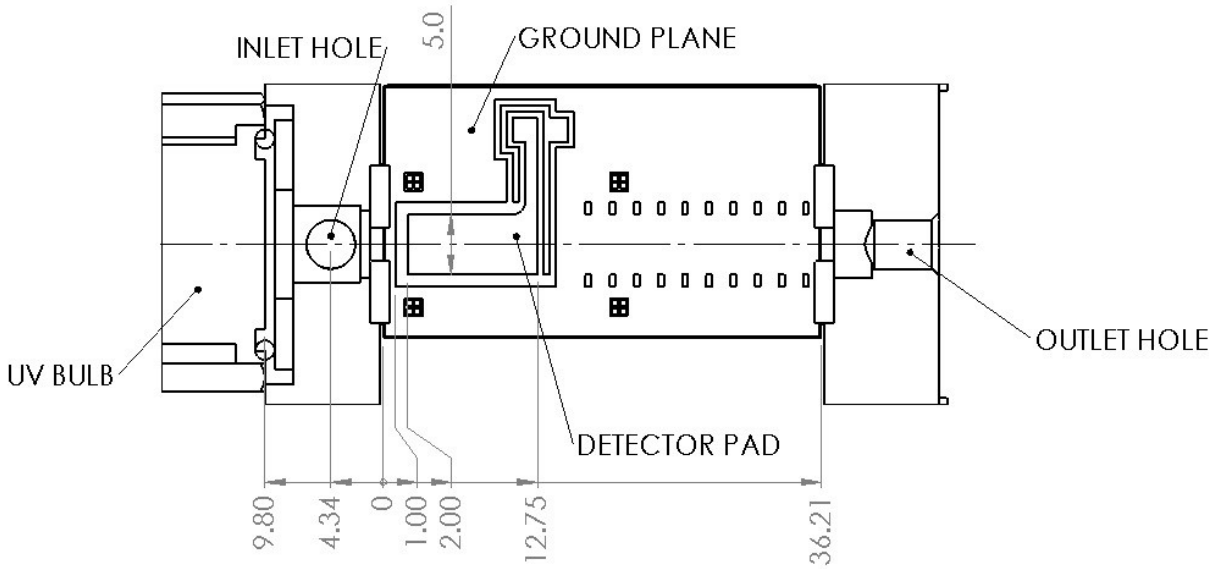

Supplemental Figure 1. Detailed dimensions (in mm) of the fixtured μDC device

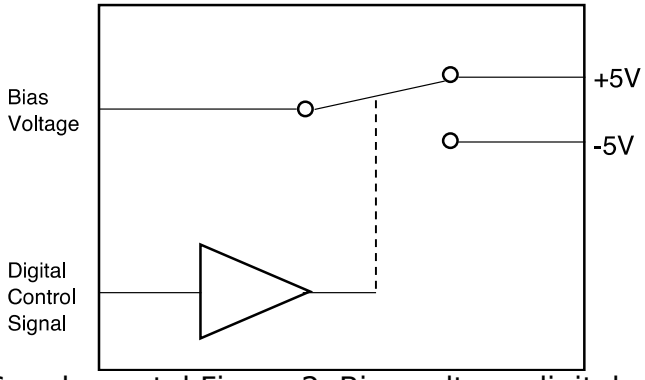

Supplemental Figure 2: Bias voltage digital selection circuit

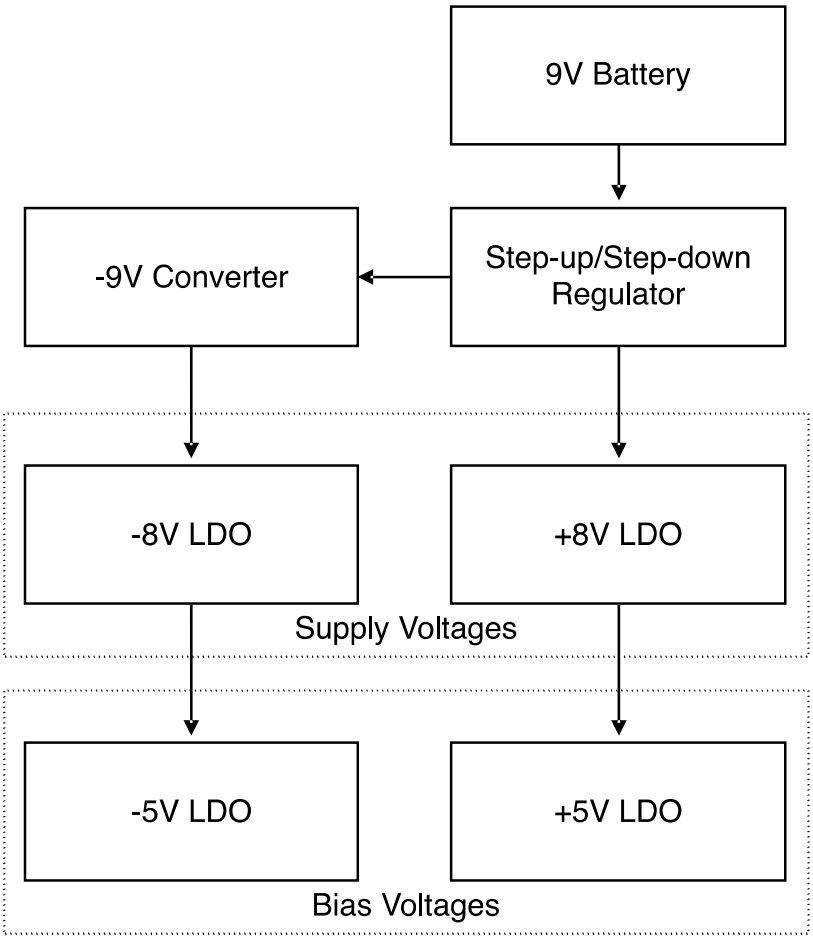

Supplemental Figure 3: Battery Power System Architecture

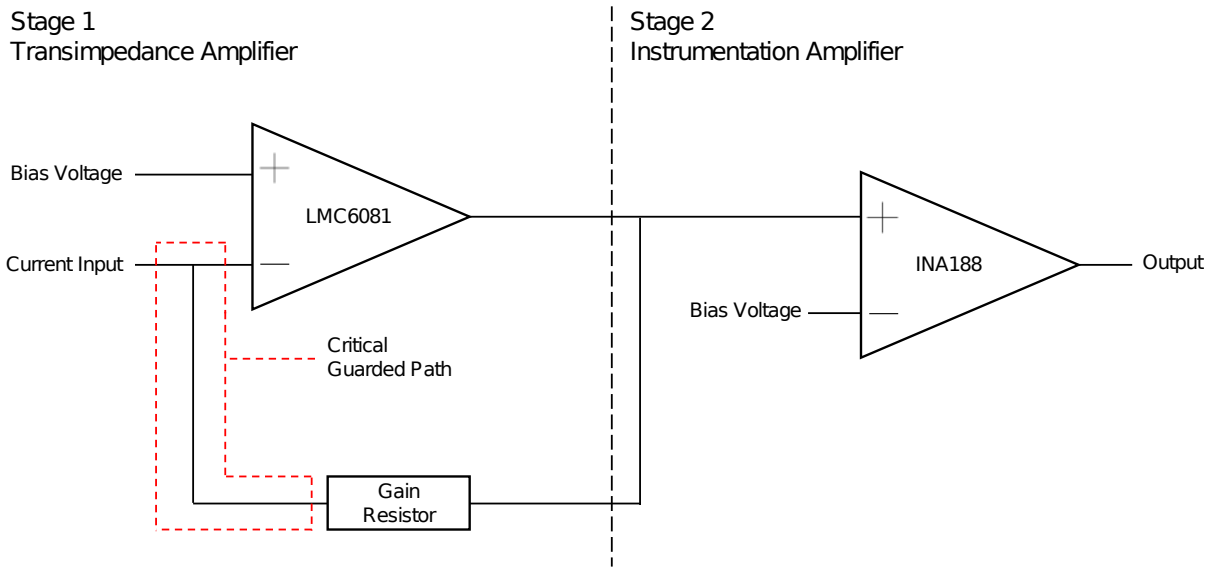

Supplemental Figure 4. Signal amplification and conditioning circuit.